Journal of Physics: Conference Series

Impact of amino acids as performance-controlling additives on the hydration of reactive MgO

Impact of amino acids as performance-controlling additives on the hydration of reactive MgO

Shuang Liang [1], Xiangming Zhou [1], Pengkun Hou [1]

[1]Department of Civil and Environmental Engineering, Brunel University London, Uxbridge, Middlesex UB8 3PH, United Kingdom

E-mail address: Xiangming.Zhou@brunel.ac.uk

Abstract. Since reactive magnesia (MgO) is produced at a lower temperature than CaO and is capable of sequestering significant quantities of CO_2, it is considered to be a technically superior and more sustainable alternative to Portland cement. To obtain maximum carbonation and associated high strength, a variety of additives are investigated for MgO. Using amino acids as an additive is a new concept to control the polymorphism of carbonates. As the hydration of magnesia plays an important role in magnesia carbonation, this study investigates the impact of amino acids (i.e. L-arginine (L-Arg) and L-aspartic (L-Asp)) on the hydration of magnesia. Subsequent tests, including X-ray diffraction (XRD), pH tests, inductively coupled plasma optical emission spectrometry (ICP-OES), thermogravimetry (TG) - differential thermogravimetry (DTG), and scanning electron microscopy-Energy-dispersive X-ray spectroscopy (SEM-EDX) were conducted after the measurement of their strength development. The results revealed that magnesia hydrated with/without amino acids only formed brucite ($Mg(OH)_2$) as the hydration product. A lower hydration degree was observed in the hydrated composites with the presence of amino acids, regardless of the type of amino acids. Specifically, the use of L-Asp not only delayed the hydration of MgO but also reduced the amount of brucite. The increasing amorphousness of brucite with increasing L-Asp concentration was also observed, compared to the control batch. Additionally, Mg^{2+} concentration was increased with the addition of L-Asp, allowing the blends to absorb more CO_2 with a higher concentration of Mg^{2+}.

1. Introduction

In the 21st century, the most significant environmental issue is the increasing CO_2 emissions to an alarming level. Traditionally, Portland cement (PC) is produced by calcining common raw materials (such as limestone and clay) at a temperature of ~1450 °C. In this process, CO_2 is released directly from the calcination of limestone ($CaCO_3$). Moreover, before calcination, $CaCO_3$ needs to be excavated and crushed, which is also an energy and carbon-intensive process. For instance, producing 1 ton cement generates 800–900 kg of CO_2, which contributes approximately 9% of worldwide anthropogenic CO_2 and 2–3% energy consumption [1,2]. From promoting sustainability point of view, more and more efforts have been made on developing alternative binders, which can reduce CO_2 emissions without sacrificing their engineering performance.

Reactive MgO cement (RMC) is considered an alternative to PC [3]. The main raw material, MgO has a lower calcination temperature (700–900 °C vs. 1450 °C) and can be entirely recycled after its lifecycle is completed [4,5]. Also, the net emissions of RMC could be further reduced by absorbing CO_2 permanently [6,7]. When reactive MgO contacts water, it forms a porous structure product, brucite ($Mg(OH)_2$), which typically has a poor strength [8]. However, the MgO-H_2O binder can gain strength through the absorption of CO_2, forming hydrated magnesium carbonates (HMCs) that can densify the microstructure of the composite and establish an outstanding binding network, becoming as strong as hydrated PC [9,10]. Since hydration and carbonation of MgO can co-occur during magnesia carbonation, therefore, it is essential to investigate the hydration of MgO before the investigation of its carbonation.

According to previous studies, the hydration of RMC can be improved by the addition of hydration agents (e.g. HCl, $MgCl_2$ and $(CH_3COO)_2Mg$) [11–14]. In terms of $MgCl_2$ and $(CH_3COO)_2Mg$, Cl^- and CH_3COO^- can migrate Mg^{2+} ions in binders away from their original particles and precipitate in the bulk solution to form brucite without covering the unhydrated particles [13]. Alternatively, the introduction of HCl decreased the pH value of the solution, creating a weak alkalinity environment, which improved the solubility of MgO and $Mg(OH)_2$ surface layer, thereby allowing the formed brucite to move away from the original particles [14]. However, few studies reported the additives that can modify the polymorphs or morphologies of RMC. It is a novel concept to control the phase polymorphs of hydrated and carbonated magnesia composites with organic matrices, while this method has been widely applied to control the properties and polymorphs of $CaCO_3$, specifically, to stabilize typically metastable calcium carbonate polymorphs including aragonite, vaterite, and amorphous calcium carbonate (ACC) [15-18].

Amino acids are hypothesized to enable the enhancement of the performance of these composites. A major advantage of amino acids as hydration agents lies in their ability to increase the concentrations of magnesium cations and carbonate anions, which can lead to the formation of HMCs early on and then facilitate the continuation of carbonation later on.

This study only aims to investigate the impact of amino acids on the hydration of MgO before the investigation of the carbonation of MgO. The mechanical performance of samples up to 14 days was investigated, and the results were further interpreted by pH measurement and characterization analysis including X-ray Diffraction (XRD), scanning electron microscopy (SEM)-Energy-dispersive X-ray spectroscopy (EDX), thermogravimetry (TG) - differential thermogravimetry (DTG) and inductively coupled plasma optical emission spectrometry (ICP-OES).

2. Experimental procedure

2.1. Materials

The reactive magnesia with a purity of > 95% by weight was sourced from Magnesia GmBH, Germany. The specific surface area (SSA) of magnesia is 0.3 m^2/g. The negatively charged L-aspartic (L-Asp) and positively charged L-arginine (L-Arg), used in this study, were obtained from Sigma Aldrich, UK.

2.2. Sample preparation

In the first step, the dry amino acids were mixed with water at concentrations of 0.1 M and 0.2 M. Afterwards, MgO powder was hand mixed with the solution or distilled water for 5 minutes at a water(solution)/solid (w/s) ratio of 0.8. The mixture containing MgO with deionized water without the presence of an amino acid was selected as a control group. The pastes were then poured into 20×20×20 mm^3 cubic moulds and gently tamped with a glass rod around 15 times to keep the consistent compaction. Immediately after casting, the cube samples were placed in a well-controlled environmental chamber, which can adjust the temperature and relative humidity (RH) very precisely to the standard saturated condition. The ambient temperature (~ 25 °C) and ambient CO_2 level (0.041 vol.% CO_2) were applied, while the RH was maintained at 95% to accelerate the hydration of MgO. Sample C-A was a control group, which was cured under an ambient environment. Samples 0.1M-A and 0.2M-A, mixed with 0.1M

L-Asp and 0.2M L-Asp solution at the same w/s ratio, were also cured under an ambient environment. Table 1 shows the mix design of each sample and their curing regimes.

Table 1. Mix formulations of MgO-H_2O (L-Asp) samples (**wt. % of the solid**) and their curing regimes

Mixture	MgO	L-Asp concentration	w/s ratio	Curing regimes
C-A	100 %	0	0.8	Ambient curing
0.1M-A	100 %	0.1 M	0.8	Ambient curing
0.2M-A	100 %	0.2 M	0.8	Ambient curing

2.3. Methodology

2.3.1. Compressive strength

A compression test was conducted at 1, 3, 7 and 14 days for three samples from each group by using an Instron 5960 universal testing machine at a loading rate of 0.4 MPa/s, which is in line with ASTM C109/C109M-13 [19]. The compressive strengths were taken as the average ones obtained from three samples.

2.3.2. pH value

According to ASTM C25 [20], the samples were ground to fine powders for measuring pH at different time intervals, from 1 to 14 days with a calibrated Mettler Toledo pH meter. 5 g of the broken sample powders were mixed with 100 g of distilled water for 30 minutes to prepare a suspension for each measurement of pH.

2.3.3. XRD, TG/DTG and SEM-EDX

XRD, TG/DTG, and SEM/EDX were conducted promptly on samples extracted from crushed cubes during the compressive test.

The XRD patterns of all samples were conducted on a Bruker D8-Advance X-ray diffractometer using Cu Kα radiation (λ=1.5418 Å). The operational voltage and the current are 40 kV and 40 mA, respectively. A scanning rate of 0.02° 2θ /step from 5 to 50° 2θ was used in this study.

TG-DTG was obtained by using a Perkin Elmer TGA 4000 equipment under nitrogen flow. The samples were heated from 20 to 1000 ºC with a heating rate of 10 ºC/min. By deconvoluting the DTG curves and calculating the area associated with each decomposition reaction under each deconvoluted curve, the various phases formed within each sample were quantified.

A Zeiss Supra 35VP SEM was used to obtain Secondary electron (SE) images, and then the images were further assessed by using an energy-dispersive X-ray (EDX) analyzer (EDAX). Before SEM analysis, a double-sided adhesive carbon disk was used to mount the dried samples onto aluminum stubs, and then the samples were coated with gold.

2.3.4. Ion concentration

5 g of MgO was added to 100 ml of either distilled water or distilled water containing 0.05 g (i.e. 1 wt. % of MgO) and 0.1 g (i.e. 2 wt.% of MgO) of L-Asp to give the suspension solution. The percentages of L-Asp by weight (1 and 2 wt.%) in the ion concentration test remained the same as those of L-Asp used in the preparation of the sample. The changes in the concentration of Mg^{2+} in the solution were carried out with a PerkinElmer Optima 2100 DV ICP-OES Spectrometer.

3. Results

3.1. XRD

Figures 1 and 2 show the MgO matrixes hydrated for up to 14 days with and without amino acids. Despite the involvement of amino acids, the observed phases are brucite ($Mg(OH)_2$) and unreacted MgO (Periclase) in all samples, indicating that amino acid only works as an inhibitor in the binders. In terms of L-Arg samples, the intensity of brucite peaks decreased with the increasing concentration of L-Arg before 7 days, demonstrating that the addition of L-Arg hinders the hydration of MgO at the first 7 days. However, this inhibiting effect began to weaken after 7 days and disappeared completely by 14 days. The amount of brucite was very close to that in all other batches at 14 days, which demonstrates the futility of L-Arg as an inhibitor.

Different from L-Arg samples, the number of brucite peaks decreased with the increasing concentration of L-Asp at all ages, showing that the addition of L-Asp obstructs the hydration of MgO during all ages. There was little MgO phase present in all batches after 14 days, which is evidence that the samples were mostly hydrated. Another interesting finding is that the intensity of brucite peaks was still low in L-Asp samples, while the periclase (MgO) peaks were negligible in all groups after 7 days, which indicates the limited formation of brucite in the samples containing L-Asp though the MgO was highly dissolved. Moreover, the amorphousness of brucite was observed to be increased with the increasing concentration of L-Asp, as determined by the observation in all curing days where the peaks became broader as the concentration of L-Asp additive increased. Compared to control samples, L-Asp-containing samples have the lower amounts and lower crystalline degree of brucite, which could be attributed to the combination of the negatively charged L-Asp and Mg^{2+}. Contrary to L-Asp-containing samples, L-Arg samples show no differences in shape from the control group, which shows that L-Arg has no effect on the crystallinity of the hydration product. Therefore, due to the outstanding impact of L-Asp on the hydration of MgO, it was selected as the benchmark amino acid in a later investigation.

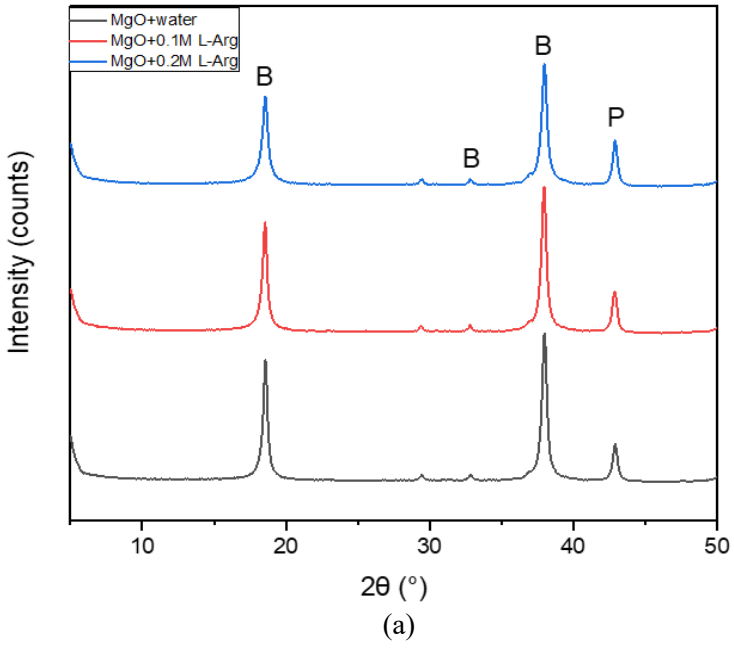

(a)

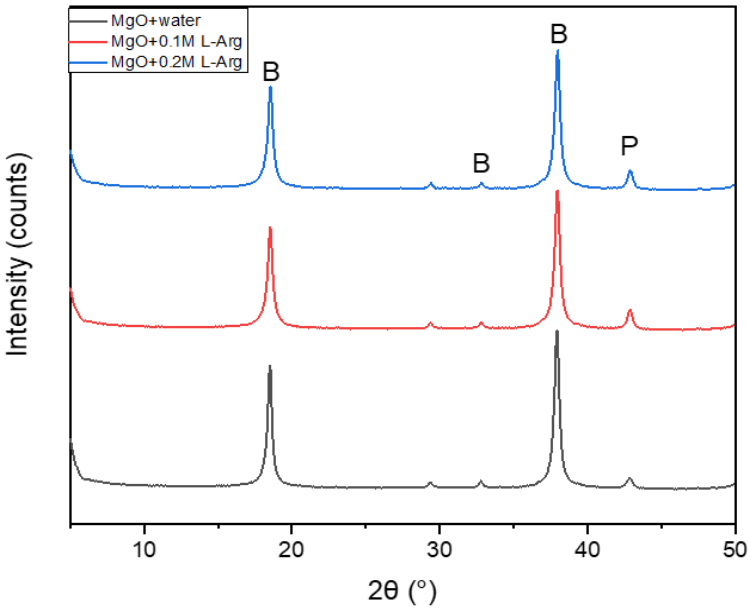
MgO+water
MgO+0.1M L-Arg
MgO+0.2M L-Arg
B
B
B
P
Intensity (counts)
10
20
30
40
50
2θ (°)

(b)

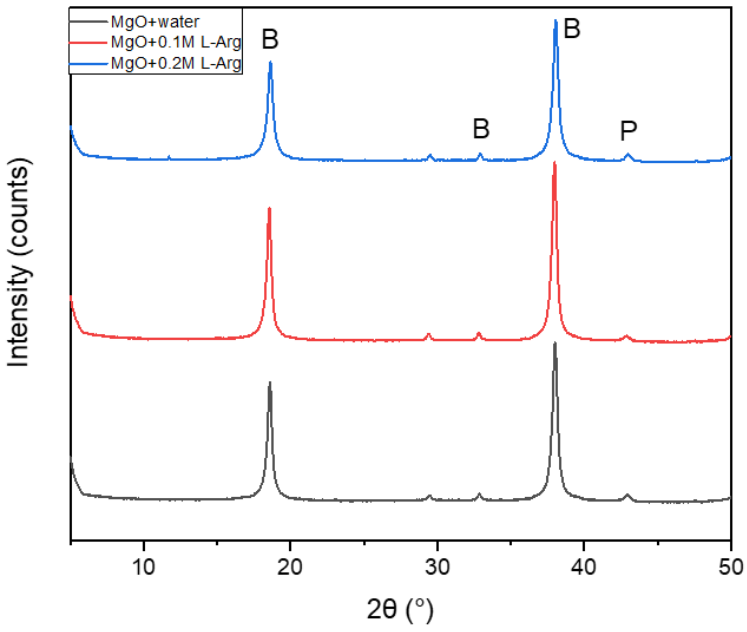
MgO+water
MgO+0.1M L-Arg
MgO+0.2M L-Arg
B
B
B
P
Intensity (counts)
10
20
30
40
50
2θ (°)

(c)

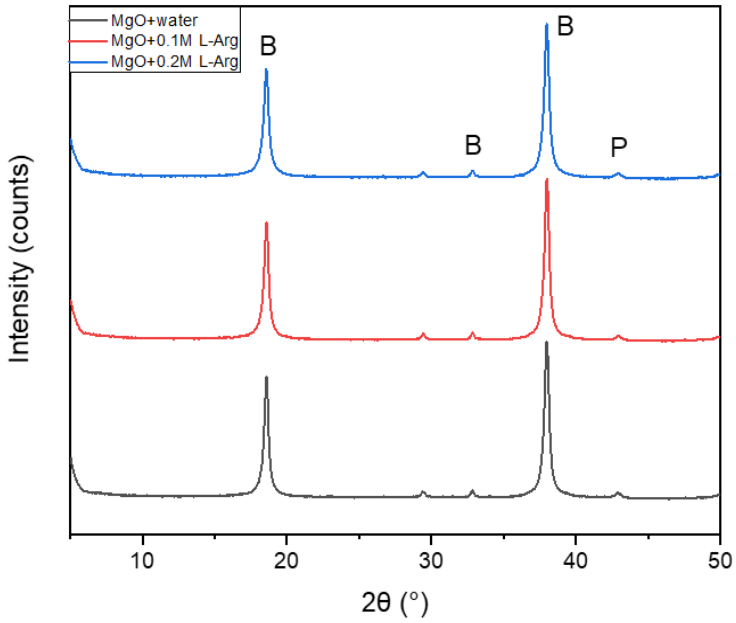

(d)

Figure 1. X-ray Diffraction patterns showing the effects of L-Arg on the hydration of MgO after (a) 1 day; (b) 3 days; (c) 7 days; (d) 14 days of ambient curing (B: Brucite; P: Periclase (MgO)).

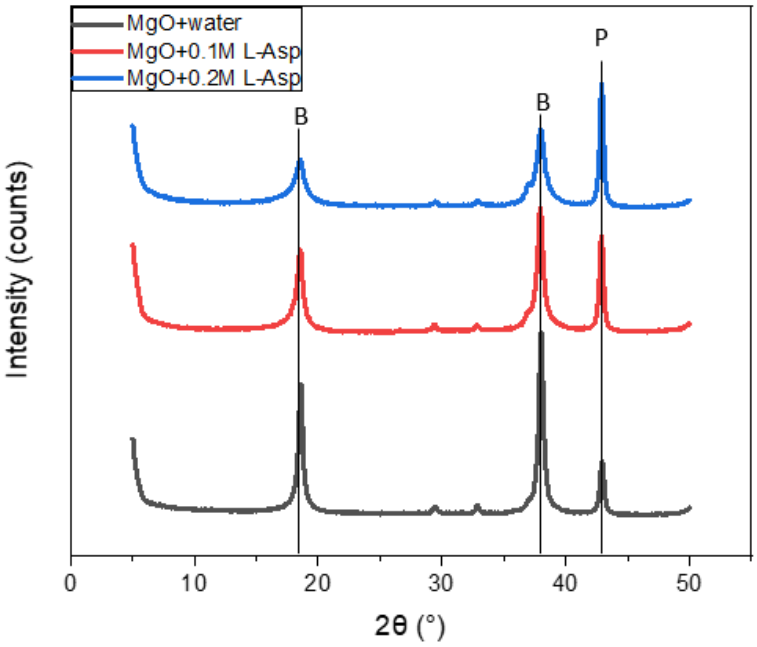

(a)

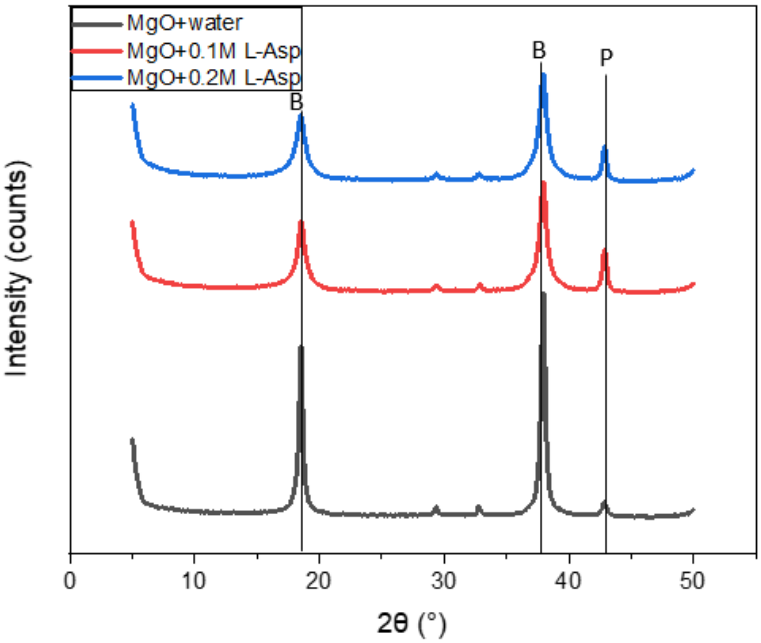
MgO+water
MgO+0.1M L-Asp
MgO+0.2M L-Asp
B
B
P
Intensity (counts)
0
10
20
30
40
50
2θ (°)

(b)

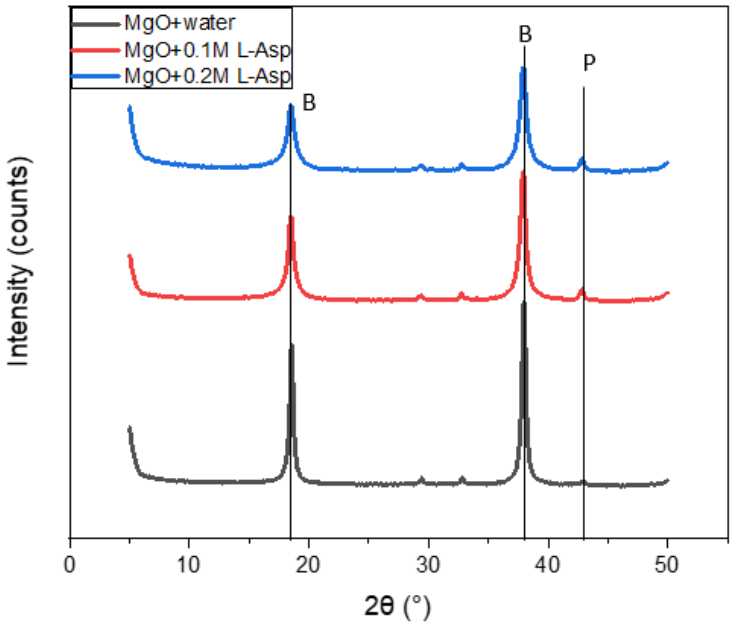
MgO+water
MgO+0.1M L-Asp
MgO+0.2M L-Asp
B
B
P
Intensity (counts)
0
10
20
30
40
50
2θ (°)

(c)

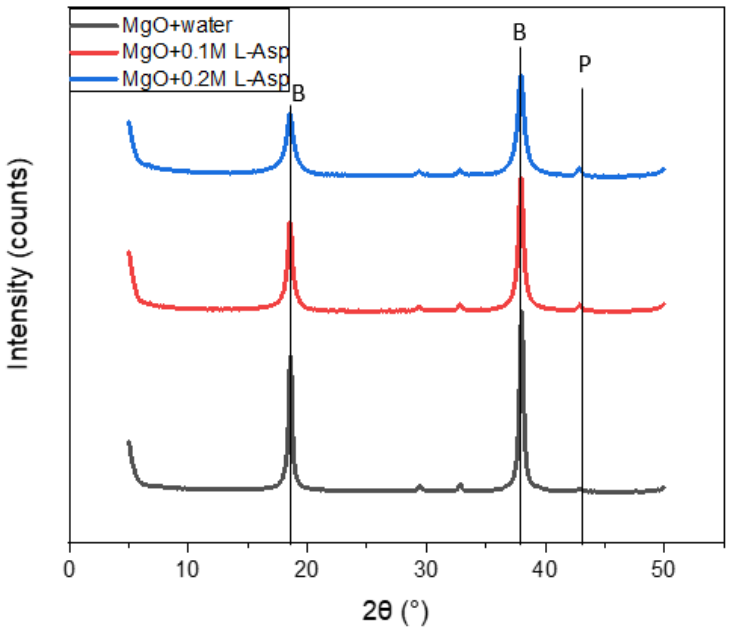

(d)

Figure 2. X-ray Diffraction patterns showing the effects of L-Asp on the hydration of MgO after (a) 1 day; (b) 3 days; (c) 7 days; (d) 14 days of ambient curing (B: Brucite; P: Periclase (MgO)).

3.2. pH values

The pH values of sample suspensions are presented in Figure 3. While a pure MgO suspension usually stabilizes at a pH of around 10.5 [21], the original pH value of the control batch is 10.6, which indicates the high purity of the raw material (i.e. MgO). When MgO contacts water, OH− anions are released and then absorbed by $Mg(OH)^+$ surface, releasing Mg^{2+} and OH^- ions into the solution. The magnesium hydroxide ($Mg(OH)_2$) precipitates on the MgO particles' surface when the ion concentration in the solution reaches the critical level (shown in equation 3.1-3.3). The introduction of L-Asp is able to retard the precipitation of OH^- ions (also shown in Figure 5), consequently, a higher pH value was observed in the L-Asp-containing samples compared to the control sample. However, at 14 days, 0.1M-A and 0.2M-A samples demonstrated lower pH values than that of the C-A sample, which could be attributed to the exhaustion of L-Asp.

$$MgO(s) + H_2O\ (l) \rightarrow Mg(OH)^+_{surface} + OH^-(aq) \quad (3.1)$$

$$Mg(OH)^+_{surface} + OH^-(aq) \rightarrow Mg(OH)^+ \cdot OH^-_{surface} \quad (3.2)$$

$$Mg(OH)^+ \cdot OH^-_{surface} \rightarrow Mg^{2+}(aq) + 2OH^-(aq) \quad (3.3)$$

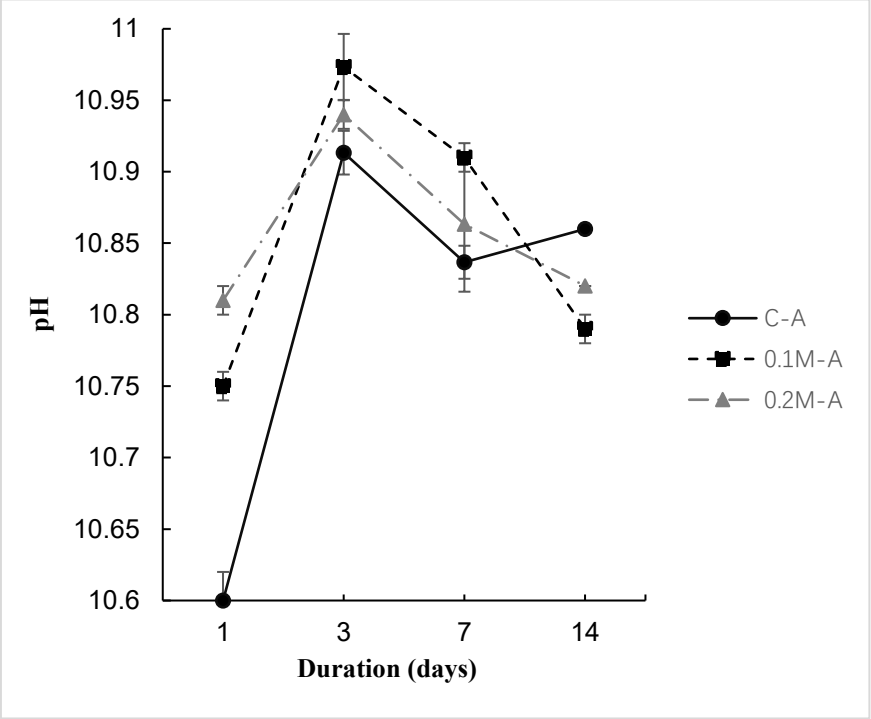

Figure 3. pH values of all samples up to 14 days

3.3. Compressive strength

Figure 4 reveals the strength gain of paste samples versus duration during 14 days of curing. As a result of limited hydration, the control sample only had a strength of ~1.9 MPa at 1 day. This sample gained its strength with the further hydration of MgO from 1 to 14 days, reaching ~3.8 MPa. The worst strength development was observed in 0.1 M L-Asp-containing samples, which only achieve ~3.2 MPa at 14 days. This poor strength development could be attributed to the less hydration product compared to the control group. Contrary to 0.1 M L-Asp samples, the compressive strengths of 0.2M L-Asp samples were ~1.9 MPa at 1 day and increased to ~2.3 MPa at 3 days, which are similar to those of C-A samples. Afterwards, the compressive strength of the 0.2 M L-Asp sample remained constant as the highest value among all samples until 14 days, despite its limited hydration product. It should be noted that the samples were prepared with a high w/s ratio at 0.8 to accelerate the hydration of MgO, therefore, MgO-based binders do not exhibit comparable mechanical properties to PC when cured at ambient condition. However, in the presence of desirable w/s ratio and accelerated carbonation conditions (as low as 5%), brucite reacts with CO_2, resulting in blocks with a 1-day strength higher than 7 MPa [22], which meets the strength requirement of commercial concrete blocks [23]. There are several key factors that influence the mechanical performance of brittle samples, such as the quantity of hydration phase formation, leading to reduced pores and more compacted structures. However, in view of the XRD patterns of the 0.2M-A and C-A samples, a higher amount of hydration phases was observed in the C-A samples compared to the 0.2M-A samples, whereas an opposite scenario was found regarding the compressive strength of the control and 0.2 M L-Asp groups, which could be interpreted by the various morphology (i.e. amorphousness) of the hydration products formed within these two groups. Hence, for the strength of the samples investigated, it is possible that the morphology of the hydration phases in the magnesium-based binder may play a greater role than their content, and previous studies also demonstrated a similar conclusion [24,25]. When MgO-based binders absorb CO_2, apart from HMCs, some unreacted brucite is also maintained in the binder. The polymorph of brucite could be modified by the application of L-

Asp, contributing more to strength than that of the crystalline brucite. Therefore, a much higher strength of the sample containing L-Asp can be expected when it is under accelerated carbonation curing.

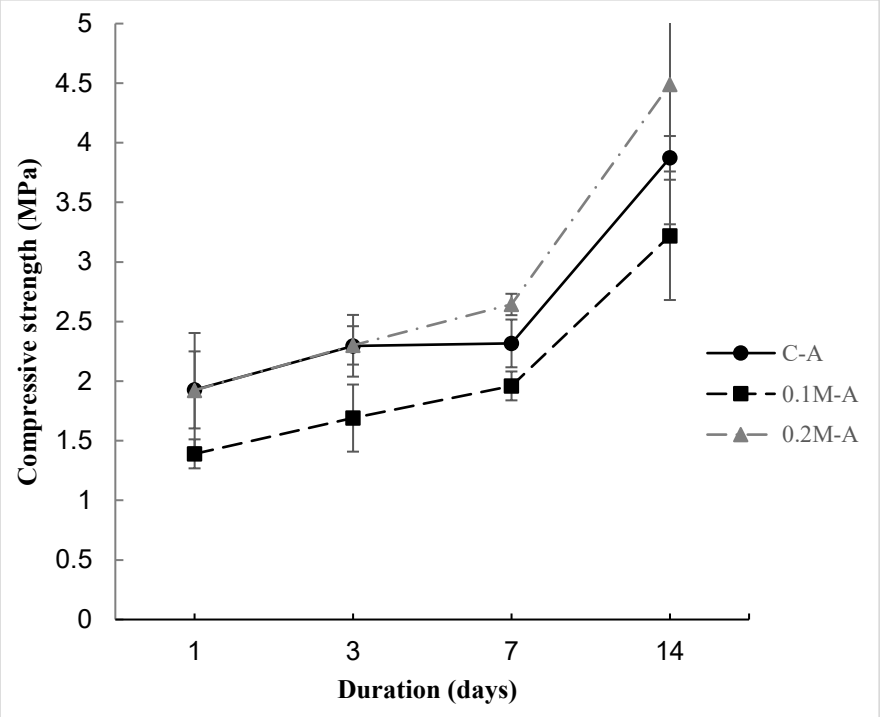

Figure 4. Compressive strength of paste samples with and without L-Asp up to 14 days

3.4. Ion concentration

The change of Mg^{2+} concentration in solution over a 6-hour hydration period is shown in Figure 5. The presence of L-Asp significantly increases the concentration of Mg^{2+} in solution by disturbing the reaction between Mg^{2+} and OH^-. The Mg^{2+} concentration in the MgO+0.05L-Asp sample deceased only after 2 hours of hydration due to the formation of brucite. However, the decrease of Mg^{2+} concentration occurred after 3 hours of hydration in the MgO+0.1L-Asp sample (i.e. 1 hour later than that of the MgO+0.05L-Asp sample), initiating the formation of brucite was delayed by the involvement of L-Asp, which agrees well with XRD results. Also, the retarded formation of brucite was proved by the higher pH values in the solution (shown in Figure 3), which exhibits the higher centration of OH^- anions in the solution.

Generally, L-Asp shows the ability to enhance both cation and anion concentrations, which has a positive impact on the future carbonation of MgO. This will be discussed in the later section (4. Discussion).

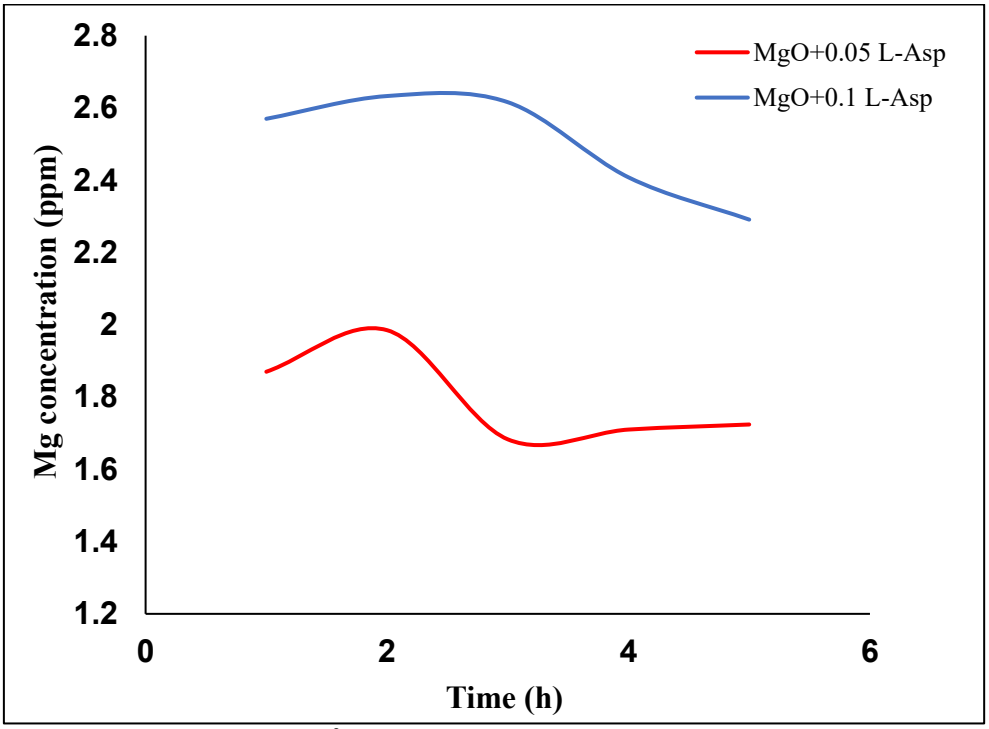

Figure 5. Changes in the total Mg^{2+} concentration in suspension with hydration age for MgO in distilled water with 0.05g and 0.1g L-Asp

3.5. TG/DTG

The mass loss results of all samples after 1 day of hydration are shown in Figure 6. C-A samples maintained the lowest amount of residue (i.e. unhydrated MgO), indicating its highest hydration degree, which agrees well with XRD results shown in Figure 2. (a). The TG data of all samples show multi-step weight loss curves for the hydration phases up to 1000 ºC. In order to determine the decomposition temperatures of each phase, the endothermic peaks on the DTG curves were studied (Figure 7). A strong endothermic peak responsible for the decomposition of formed brucite was observed at around ~200–550°C, indicating the high amount of hydration phase in the blend. According to DTG curves, the three stages of mass loss involved during thermal decomposition can be summarized as follows:

50-200 ºC: Mass loss due to the loss of bonding water in the mixture.

200-550 ºC: Mass loss due to the decomposition of uncarbonated brucite.

550-1000 ºC: Decarbonation of HMCs.

As shown in Table 2, the areas obtained by the deconvolution of DTG results were used to calculate the certain mass loss, which was related to the decomposition of all hydrate/carbonate phases. According to a study [26], it is hypothesised that the poorly crystalline phases in magnesia blends can be represented by the additional bonding water. The mass loss at ~ 90 °C in samples 0.1M-A and 0.2M-A are higher than that of the C-A sample, which further proved this hypothesis. Also, poorly crystalline phases in samples containing L-Asp could be observed by the XRD results (Figure 2) and SEM images (Figure 9. (b)). Compared to 0.1M-A and 0.2M-A samples, the C-A sample shows the highest mass loss (26% and 23.4% vs. 28.8%) at 200-550 °C, suggesting the largest amount of hydration phase (i.e. brucite), which is in line with the XRD results. Even though the C-A sample contained the most hydration product, it showed an undesirable mechanical performance, which proves that the amount of hydration phase is not the only reason to affect the strength. The weight loss between 550 to 1000 °C of the 0.2M-A sample (3.9%) is much higher than that of the samples 0.1M-A (2.6%) and C-A (2.4%), possibly showing its substantially higher carbonation degree of magnesia, which exhibits the potential of L-Asp to improve the carbonation degree of the magnesia-based binder.

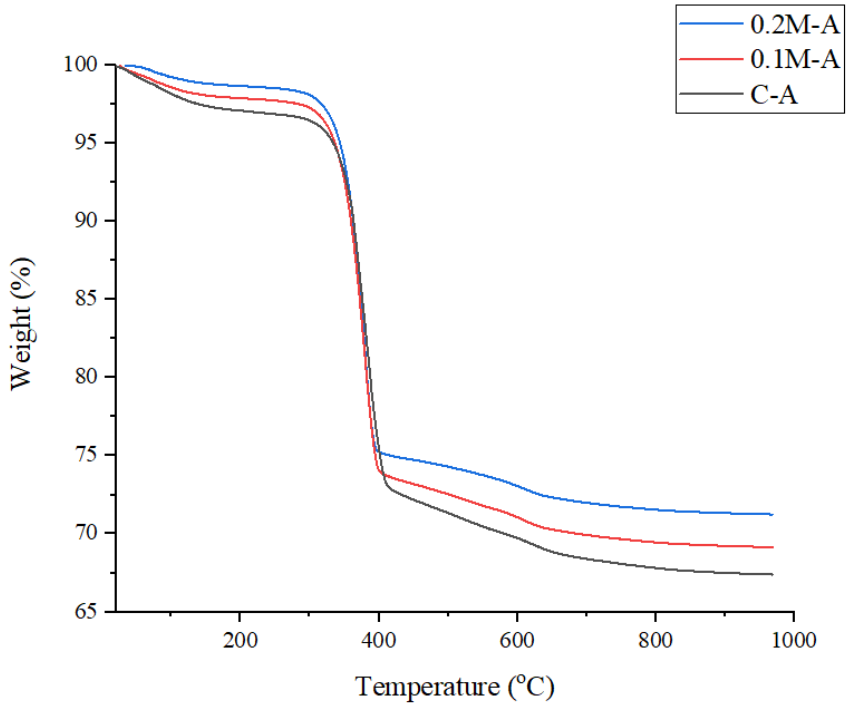

Figure 6. TG results of all samples after 1 day of curing

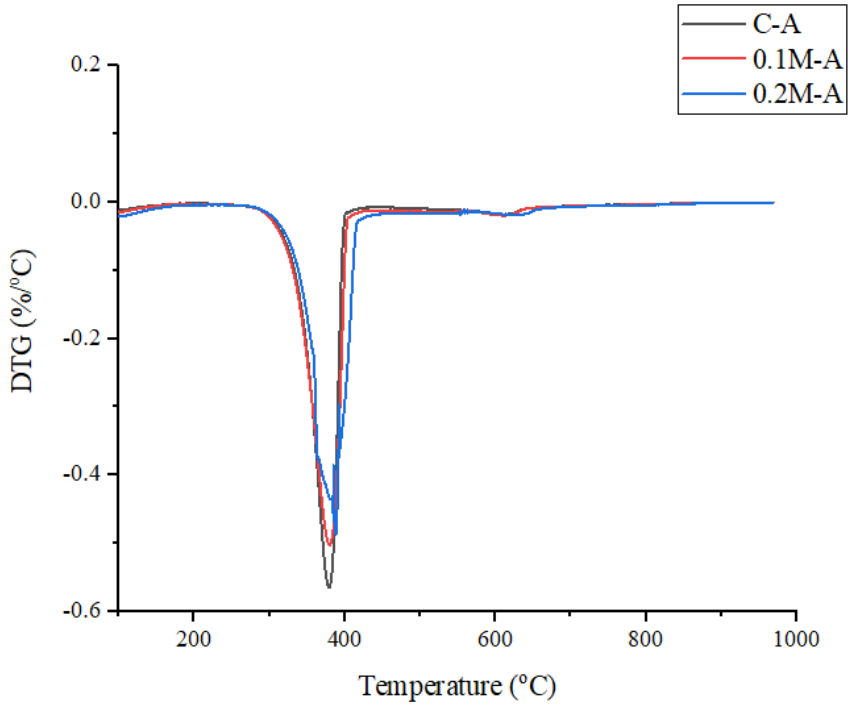

Figure 7. DTG results of all samples after 1 day of curing

Table 2. Mass loss (wt.%) of samples analyzed at 1 day by thermogravimetric analysis

Mixture	50-200ºC	200-550ºC	550-1000ºC
C-A	1.3	28.8	2.4

0.1M-A	2.1	26	2.6
0.2M-A	1.4	23.4	3.9

3.6. SEM-EDX

Considering the elemental spectra in Figure 8, the only hydration product is brucite, which reveals the reaction of MgO under an ambient environment, and the formed hydration phases (i.e. brucite) account for its strength improvement, and the results are also in line with XRD patterns and mechanical performance. The morphologies of the hydration products of C-A and 0.2M-A samples after 14 days are shown in Figure 9. The morphology of brucite in 0.2M-A samples was significantly changed by the use of L-Asp. Different morphologies can be observed in the SEM images, and the brucite with a hexagonal crystal structure was formed through the hydration of the control sample. The C-A sample exhibited the lowest compressive strength due to the weak connection observed in the hexagonal brucite crystals. Interestingly, with the involvement of L-Asp, the brucite particles tended to be spherical, indicating their higher amorphousness. The noticeable improvement in compressive strength of 0.2M-A samples could be attributed to the densification of the microstructure, which is composed of hydration phases with improved morphologies.

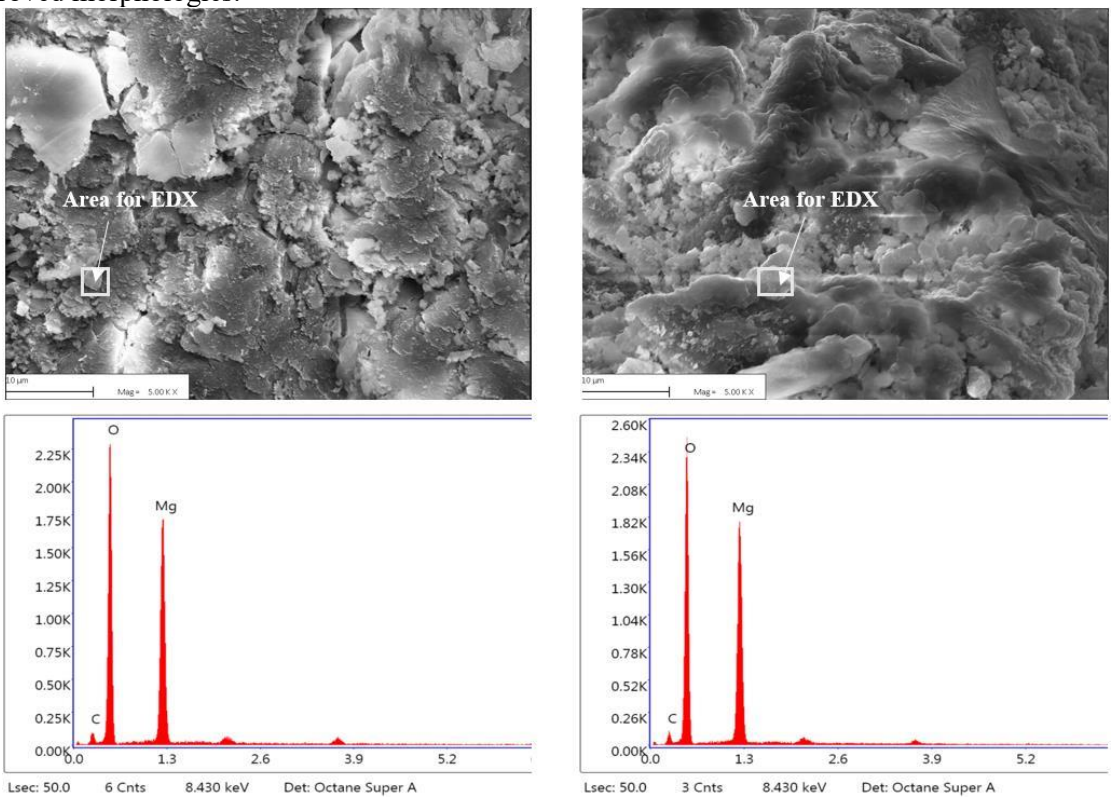

(a) (b)

Figure 8. Elemental spectra of selected areas in (a) C-A (magnification: x5000) and (b) 0.2M-A (magnification: x5000)

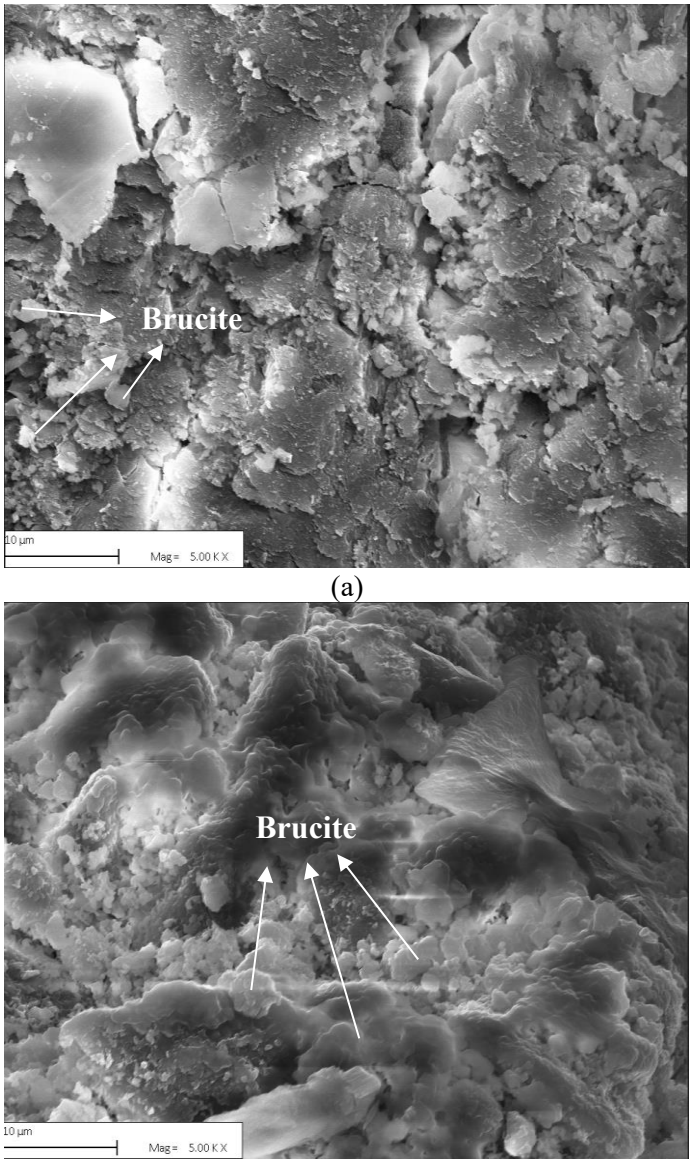

Figure 9. SEM images of (a) C-A (magnification: x5000); (b) 0.2M-A (magnification: x5000) after 14 days of curing

4. Discussion

The continuous hydration of MgO led to the formation of brucite, which connected the unhydrated particles, explaining the strength development. With the use of L-Asp, the type of hydration phase does not change, but only the amount of hydration phase has been changed. Normally, the higher the hydration product content, the higher the strength. However, a contrary scenario was observed in this study, with the involvement of L-Asp, the formed amorphous brucite, together with hexagonal brucite, led to a greater strength improvement in the 0.2M-A samples compared with that in the C-A group. One explanation is that the hydration phases in the 0.2M-A samples provide better microstructure which is related to their strong and dense nature. Besides, it is reported that amorphous gel-like growths are more

useful than hexagonal or tabular crystals in terms of strength improvement as a result of the structures of amorphous phases [27], indicating that the morphology, rather than the amount, of hydration phases, plays a more important role in the determination of strength development in samples investigated.

Moreover, the ion concentration in the paste has also been modified by the L-Asp. When using L-Asp, a large amount of free Mg^{2+} and OH^- ions were maintained in the paste without precipitation, which is highly desirable for the carbonation of MgO. The high concentration of OH^- in the paste leads to a high pH environment, which is helpful to dissolve the CO_2, and for producing HCO_3^- and CO_3^{2-}. Afterwards, the high amount of Mg^{2+} ions can react with HCO_3^- and CO_3^{2-} to form the HMCs, further increasing the mechanical strength and improving the microstructure of the magnesia-based samples.

5. Conclusions

The major observations of this study are listed below:

The addition of L-Arg only reduces the amount of hydration phase (i.e. brucite) prominently at the early ages (before 3 days curing), then the effectiveness of L-Arg was exhausted at 14 days. Also, L-Arg failed to alter the polymorphs of the hydration product.

The use of L-Asp reduces the amount of hydration phase, leading to the formation of brucite with high amorphousness, which has a positive contribution to the strength. The MgO-H_2O composites containing 0.2M L-Asp showed up to a 16% increase in compressive strength at 14 days, compared to the control batch. L-Asp highly changes the morphology of the product and densifies the microstructure of magnesia-based samples. The strength of the samples may be affected more by the morphology of hydration products than by their amount.

The introduction of L-Asp is able to retard the precipitation of Mg^{2+} and OH^-, consequently, the higher concentrations of Mg^{2+} and OH^- were observed in the L-Asp-containing samples compared to the control sample, which provides the potential to improve the carbonation of MgO.

Acknowledgement

The authors would like to thank Zhongyuan University of Technology for providing partially a PhD studentship to the first author for conducting this research at Brunel University London and thank Brunel University London to provide a travel grant to the first author to present this paper at the 5th International Conference on Innovative Materials, Structures and Technologies.

References

[1] Olivier, J. G., J. A. Peters and G. Janssens-Maenhout 2012 Trends in global CO2 emissions 2012 report The Netherlands, PBL Netherlands Environmental Assessment Agency.
[2] Juenger, M. C. G., F. Winnefeld, J. L. Provis and J. H. Ideker 2011 Advances in alternative cementitious binders Cem. Concr. Res. 41(12): 1232-1243.
[3] S.A. Walling, J.L. Provis 2.16 Magnesia-based cements: a journey of 150 years, and cements for the future? Chem. Rev. 116 4170–4204, https://doi.org/10. 1021/acs.chemrev.5b00463.
[4] A. Al-Tabbaa 2013 19 - Reactive magnesia cement, in: F. Pacheco-Torgal, S. Jalali, J. Labrincha, V.M. John (Eds.) Eco-Efficient Concrete, Woodhead Publishing, 2013, pp. 523-543.
[5] K. Hirota, N. Okabayashi, K. Toyoda, O. Yamaguchi 1992 Characterization and sintering of reactive MgO Mater. Res. Bull. 27 (1992) 319–326
[6] R. Hay, K. Celik 2020 Accelerated carbonation of reactive magnesium oxide cement (RMC)-based composite with supercritical carbon dioxide (scCO2) J. Cleaner Prod. 248 119282.
[7] E. Gartner, T. Sui 2018 Alternative cement clinkers, Cem. Concr. Res. 114 27– 39.
[8] X. Li 2012 Mechanical Properties and Durability Performance of Reactive Magnesia Cement Concrete University of Cambridge, 2012.
[9] L. Mo, D.K. Panesar 2012 Effects of accelerated carbonation on the microstructure of Portland cement pastes containing reactive MgO, Cem. Concr. Res. 42 769–777.
[10] D.A. Torres-Rodríguez, H. Pfeiffer 2011 Thermokinetic analysis of the MgO surface carbonation process in the presence of water vapor, Thermochim Acta 516 74–78.
[11] N.T. Dung, C. Unluer 2017 Carbonated MgO concrete with improved performance: the influence of temperature and hydration agent on hydration, carbonation and strength gain Cem. Concr. Compos. 82 (2017) 152–164.
[12] N.T. Dung, C. Unluer 2017 Sequestration of CO2 in reactive MgO cement-based mixes with enhanced hydration mechanisms Constr. Build. Mater. 143 71–82.
[13] E.M. van der Merwe, C. Strydom, A. Botha 2004 Hydration of medium reactive industrial magnesium oxide with magnesium acetate J. Therm. Anal. Calorim. 77 49–56.
[14] K.P. Matabola, E.M. van der Merwe, C.A. Strydom, F.J.W. Labuschagne 2010 The influence of hydrating agents on the hydration of industrial magnesium oxide J. Chem. Technol. Biotechnol. 85 1569–1574.
[15] L. Ma, J. Zhu, M. Cui, L. Huang, Y. Su 2015 Biomimetic synthesis of novel calcium carbonate heterogeneous dendrites New J. Chem. 39 5309–5315, https:// doi.org/10.1039/c5nj00219b.
[16] K. Maruyama, T. Yoshino, H. Kagi 2011 Synthesizing a composite material of amorphous calcium carbonate and aspartic acid Mater. Lett. 65) 179–181, https://doi.org/10.1016/j.matlet.2010.09.039.
[17] Z. Zou, L. Bertinetti, Y. Politi, P. Fratzl, W.J.E.M. Habraken 2017 Control of polymorph selection in amorphous calcium carbonate crystallization by poly (aspartic acid): two different mechanisms Small. 13 1–11, https://doi.org/10.1002/ smll.201603100.
[18] N.A.J.M. Sommerdijk, G. De With 2008 Biomimetic CaCO3 mineralization using designer molecules and interfaces Chem. Rev. 108 (11) 4499–4550.
[19] ASTM, C109-13A 2013 Standard test method for compressive strength of hydraulic cement mortars ASTM, Philadelphia, PA, USA, 2013.
[20] ASTM, C25-06 2019 Standard test methods for chemical analysis of limestone, quicklime and hydrated lime, ASTM International, West Conshohocken, PA, Vol. 10, 2019.
[21] F. Jin, A. Al-Tabbaa 2014 Strength and hydration products of reactive MgO–silica pastes, Cem. Concr. Compos. 52 27–33.
[22] Unluer, C. and A. Al-Tabbaa 2014 Enhancing the carbonation of MgO cement porous blocks

through improved curing conditions Cem. Concr. Res. **59**: 55-65.
[23] British Standard-771-4, E 2011 Specification for masonry units. Aggregate concrete masonry units (dense and light-weight aggregates). UK.
[24] P. De Silva, L. Bucea, V. Sirivivatnanon 2009 Chemical, microstructural and strength development of calcium and magnesium carbonate binders Cem. Concr. Res. 39 (5) 460–465
[25] Ruan, S., Liang, S., Kastiukas, G., Zhu, W., & Zhou, X 2020 Solidification of waste excavation clay using reactive magnesia, quicklime, sodium carbonate and early-age oven curing. Constr. Build. Mater. 258, 120333.
[26] F. Winnefeld, E. Epifania, F. Montagnaro, E.M. Gartner 2019 Further studies of the hydration of MgO-hydromagnesite blends, Cem. Concr. Res. 126 105912.
[27] Hoang, T., Dung, N. T., Unluer, C., & Chu, J 2021 Use of microbial carbonation process to enable self‐carbonation of reactive MgO cement mixes Cem. Concr. Res. 143, 106391.